

Giant room-temperature barocaloric effects in PDMS rubber at low pressures

A. M. G. Carvalho^{1,*}, W. Imamura^{1,2}, E. O. Usuda¹ and N. M. Bom¹

¹ *Laboratório Nacional de Luz Síncrotron, CNPEM, 13083-970, Campinas, SP, Brazil.*

² *Faculdade de Engenharia Mecânica, UNICAMP, 13083-860, Campinas, SP, Brazil.*

* E-mail: alexandre.carvalho@lnls.br

ABSTRACT

The barocaloric effect is still an incipient scientific topic, but it has been attracting an increasing attention in the last years due to promising perspectives for application in alternative cooling devices. Here, we present giant values of barocaloric entropy change and temperature change induced by low pressure changes in the PDMS elastomer around room temperature. We report an entropy change of $69 \text{ J kg}^{-1} \text{ K}^{-1}$ for a pressure change of 130 MPa; and temperature changes of 12.0 K and 28.5 K, for pressure changes of 173 MPa and 390 MPa, respectively. A huge normalized temperature change of $\sim 70 \text{ K GPa}^{-1}$ was observed in a large temperature range. We found barocaloric effect values that exceed those previously reported for any promising barocaloric materials around room temperature. Our results stimulate the study of the barocaloric effect in elastomer polymers and broaden the pathway to use this effect in solid-state cooling technologies.

In the beginning of the nineteenth century, John Gough detected and described the heating of natural rubber when rapidly stretched¹. This effect was further studied by Joule, reporting temperature changes induced by uniaxial stress in different materials, including rubbers, metals, and woods². In fact, both scientists described what we designate elastocaloric effect (σ_e -CE), the first *i*-caloric effect ever reported. *i*-caloric effects (“*i*” stands for intensive thermodynamics variables) can be characterized by the adiabatic temperature change (ΔT_S) and the isothermal entropy change (ΔS_T) induced by an external field applied on a material.

Besides the magnetocaloric effect (h -CE) and the electrocaloric effect (e -CE), Lord Kelvin³ also predicted the barocaloric effect (σ_b -CE), which should be driven by isotropic stress variations. As well as h -CE and e -CE, the barocaloric effect may be used in solid-state cooling devices through a cooling cycle, as illustrated in Fig. 1. Both σ_b -CE and σ_e -CE are facets of the mechanocaloric effect (σ -CE). The research into *i*-caloric effects has blossomed in the last decades, as a consequence of the experimental demonstration of the giant h -CE⁴ and the giant e -CE⁵, leading to significant advances in materials and prototypes. Despite the interesting results obtained by stretching natural rubber (NR) and other polymers in the 1940 decade⁶⁷, the σ -CE is the least studied *i*-caloric effect, contrasting the large number of papers on h -CE and e -CE. Nevertheless, recently, there was a resurgence of σ -CE due the practicality of applying mechanical stress in comparison to magnetic or electrical fields.

Giant values of σ_e -CE and σ_b -CE around room temperature were reported in shape-memory alloys (SMAs) based on Cu-Zn-Al ($\Delta S_T = -22 \text{ J kg}^{-1} \text{ K}^{-1}$ at 295 K, for a pressure change $\Delta\sigma = 143 \text{ MPa}$)⁸ and Ni-Mn-In ($\Delta S_T = -24.4 \text{ J kg}^{-1} \text{ K}^{-1}$ and $\Delta T_S = 4.5 \text{ K}$ at 293 K, for $\Delta\sigma = 260 \text{ MPa}$)⁹, respectively. Other examples of giant σ -CE around room temperature are observed in $\text{Ni}_{46}\text{Mn}_{38}\text{Sb}_{12}\text{Co}_4$ ¹⁰ and $\text{Fe}_{49}\text{Rh}_{51}$ ¹¹. Below room temperature, $(\text{NH}_4)_2\text{SO}_4$ presents promising barocaloric properties (obtained indirectly)¹². Based on good potential of SMAs, a regenerative elastocaloric heat pump was reported recently¹³.

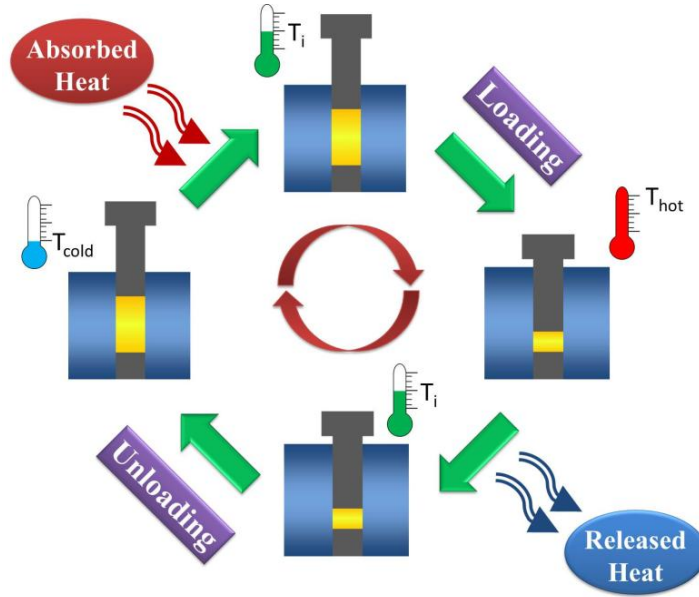


Fig. 1: Scheme of a four-stage barocaloric cycle based on loading/unloading process. The yellow rectangles represent the solid refrigerant during the cycles. As a first step, the material is adiabatically compressed, increasing the sample temperature (T_{hot}). Then, while the applied pressure is kept constant, the heat gradually flows out from the sample to heat sink and the temperature decreases down to initial temperature (T_i). In the third step, the load is adiabatically released and the sample is cooled down (T_{cold}). Finally, the sample absorbs heat from the surroundings and returns to T_i .

Alternatively to SMAs, polymers have also attracted some attention regarding the σ -CE^{14,15,16,17,18,19,20}. Elastomer polymers have shown to be particularly suitable for mechanocaloric applications, since it presents good results concerning fatigue properties combined with high caloric potential²¹. Moreover, all elastomers can act as mechanocaloric materials due the contribution of polymer chains rearrangement, not depending on phase transitions (as in the case of ferroics). The research on σ_e -CE¹⁸ and σ_b -CE²⁰ is still in the beginning, with plenty of unexplored possibilities.

In this context, the polydimethylsiloxane rubber (PDMS) appears as a potential mechanocaloric material. PDMS is an elastomer composed of long-chain molecules with freely rotating links, weak secondary forces between the molecules, and crosslinks able to form a three-dimensional network²². Moreover, PDMS is also amorphous around room temperature. Combining these particularities with the compression process via confined compression, we can hypothesize that the entropy or the temperature can be changed more easily in PDMS than in other non-rubber-like solids (e.g., SMAs). Therefore, we have systematically investigated the σ_b -CE in PDMS around room temperature at relatively low pressures. Our experiments reveal that PDMS exhibits

giant temperature and entropy variations, presenting a better performance in comparison with all other mechanocaloric materials studied so far.

Firstly, we measured the temperature changes of the PDMS rubber for different pressure variations (Fig. 2a). We observe a thermal giant σ_b -CE of 27.7 K at ~ 283 K, for $\Delta\sigma = 390$ MPa (compression), and the temperature change $\Delta T = -28.5$ K, at the same temperature, for $\Delta\sigma = -390$ MPa (decompression). The difference between the values of ΔT in compression and decompression processes, for the highest pressure variations that we measured, is due to the fact that the decompression process is closer to the adiabatic condition than the compression process. Taking the process $0 \text{ MPa} \rightarrow 390 \text{ MPa} \rightarrow 0 \text{ MPa}$ as an example, the temperature relaxation during compression has a time constant of $\tau_{\text{comp}} = 19.1$ s, while the time constant is $\tau_{\text{decomp}} = 24.6$ s for decompression. Then, if $\tau_{\text{comp}} < \tau_{\text{decomp}}$ and the specific heat of the sample does not change significantly during compression and decompression processes, the heat transfer rate for compression is larger than decompression.

Fig. 2b displays the ΔT as function of temperature in decompression process within the 26.0(5) - 390(12) MPa pressure range. At 303 K, for example, it was obtained a ΔT of -12.1 K for just 173(3) MPa, higher than observed for V-NR in the same conditions ($\Delta T = -10.5$ K at 303 K, for $\Delta\sigma = -173(3)$ MPa)²⁰. Furthermore, PDMS rubber at low temperatures (223 and 243 K) was also analyzed for pressure changes of 43.4(9) and 173(3) MPa, demonstrating high ΔT even below room temperature. This behavior is interesting since ΔT does not change significantly in a wide temperature range (i.e., ΔT does not fall abruptly as in magnetocaloric compounds²³ or SMAs^{24,25,26}).

For several materials that present i -caloric effects, the maximum magnitude of the ΔT_S increases as a function of the maximum applied field, following a power law of the type $\Delta T_S(T, i) = ai^n$. For example, the external field in the magnetocaloric effect (h -CE) is the magnetic field (H), and $n = 2/3$ around the magnetic transition. In this case, ΔT_S and ΔS_T are proportional to $H_{\text{max}}^{2/3}$, which is predicted from the Mean Field Theory²⁷ and observed experimentally. For electrocaloric effect (e -CE), a power law was reported for a ferroelectric polymer, for which $n = 2$ (i.e., $\Delta T_S \propto E_{\text{max}}^2$) at low electric fields (E), and $n = 2/3$ at higher E (i.e., $\Delta T_S \propto E_{\text{max}}^{2/3}$)²⁸. Following this concept, Usuda et al.²⁰ also proposed a power law for σ_b -CE:

$$|\Delta T(T, \sigma_{\text{max}})| = a\sigma_{\text{max}}^n, \quad (1)$$

where a is the constant of proportionality, and σ_{max} is the maximum value of the released pressure. The fitted model for PDMS rubber at 263 K is shown in Fig. 2c. In this case, $a = 62(5)$ K GPa ^{n} , and $n = 0.90(6)$. For other temperatures (fits not shown), we found: $a = 56(4)$ K GPa ^{n} and $n = 0.88(6)$ for 243 K; $a = 73(7)$ K GPa ^{n} and $n = 0.98(8)$ for 283 K; and $a = 69(6)$ K GPa ^{n} and $n = 0.94(6)$ for 303 K. As an informative comparison, the same parameters for vulcanized natural rubber (V-NR) at 283 K are $a = 51(3)$ GPa ^{n} K and $n = 0.94(3)$ ²⁰. Either for PDMS or V-NR, ΔT vs. σ_{max} could be fitted using a power law. For PDMS, the parameters a and n tend to increase slightly as temperature increases.

The strain, defined as $\varepsilon \equiv \Delta l/l_0$ (where Δl is length change of the sample and l_0 is the initial length), was measured as a function of temperature during cooling isobaric processes (Fig. 3a), in order to obtain the isothermal entropy change (ΔS_T) as a function of temperature (Fig. 3b), through the following equation:

$$\Delta S_T(T, \Delta\sigma) = -\frac{1}{\rho_0} \int_{\sigma_1}^{\sigma_2} \left(\frac{\partial \varepsilon}{\partial T} \right)_{\sigma} d\sigma, \quad (2)$$

where ρ_0 is the density of the sample at atmospheric pressure, and σ_1 and σ_2 are initial and final pressures, respectively²⁰. At 290 K, we obtained a giant σ_b -CE of $-69(7)$ J kg⁻¹ K⁻¹ for merely $\Delta\sigma = 130(3)$ MPa. This leads to a normalized entropy change of $0.53(6)$ kJ kg⁻¹ K⁻¹ GPa⁻¹. For $\Delta\sigma = 87(2)$ MPa, the entropy change is lower, $-47(5)$ J kg⁻¹ K⁻¹, but the normalized entropy change keeps its high value: $0.54(6)$ kJ kg⁻¹ K⁻¹ GPa⁻¹. It is clear that, for the highest pressure changes, ΔS_T has the tendency of keeping increasing at temperatures below 290 K. Moreover, PDMS rubber also exhibits an inverse σ_b -CE at higher temperatures (e.g., inverse σ_b -CE begins to appear for $\Delta\sigma = 130(3)$ MPa above $T_{inv} \approx 316$ K); as $\Delta\sigma$ decreases, the temperature T_{inv} , that marks the inversion of the σ_b -CE in PDMS, shifts to higher values.

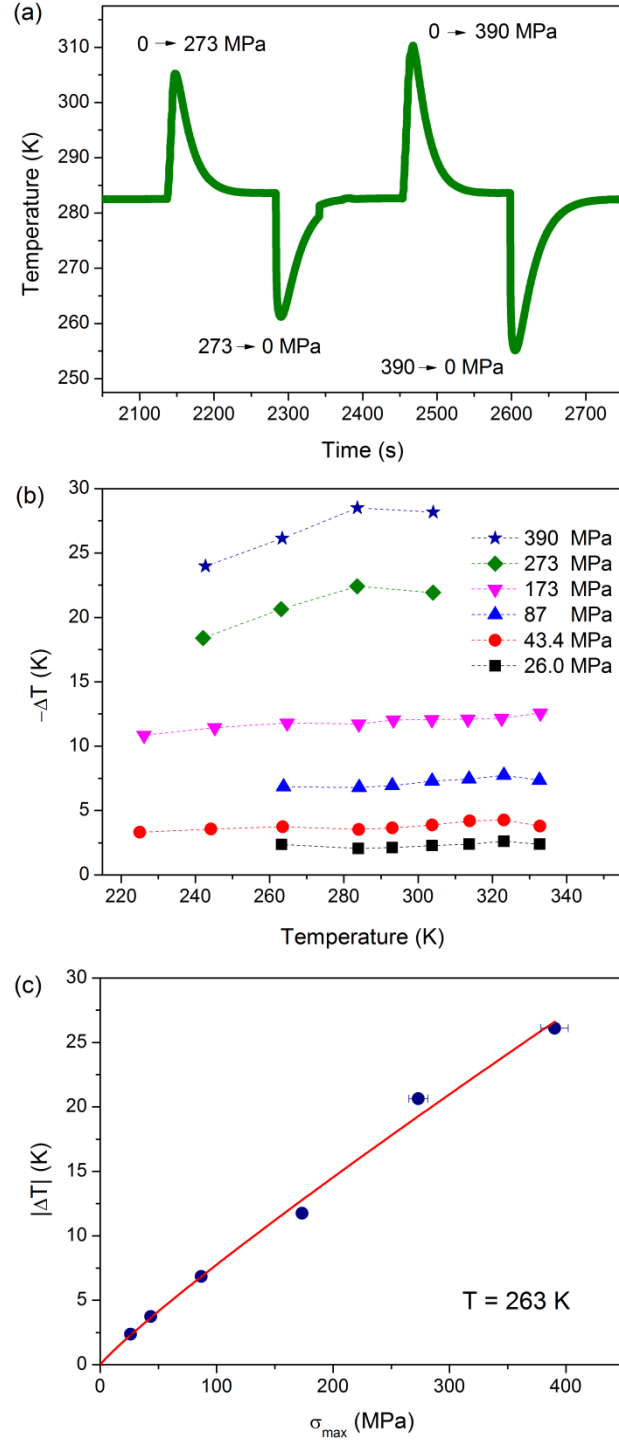


Fig. 2: (a) Temperature vs. time for PDMS rubber at initial temperature of ~ 283 K; the peaks (or the valleys) are related to the temperature change when the pressures of 273(8) and 390(12) MPa are applied (or released). (b) Temperature change vs. initial temperature for decompression process at different pressures (26.0(5), 43.4(9), 87(2), 173(3), 273(8) and 390(12) MPa); the dotted lines connecting the symbols are guides for the eyes. (c) Modulus of temperature change vs. released pressure for initial temperature of 263 K; the circles are experimental data, and the line is the fits using Eq. 1; we estimate an error of 2% for pressures up to 173 MPa and 3% above 173 MPa.

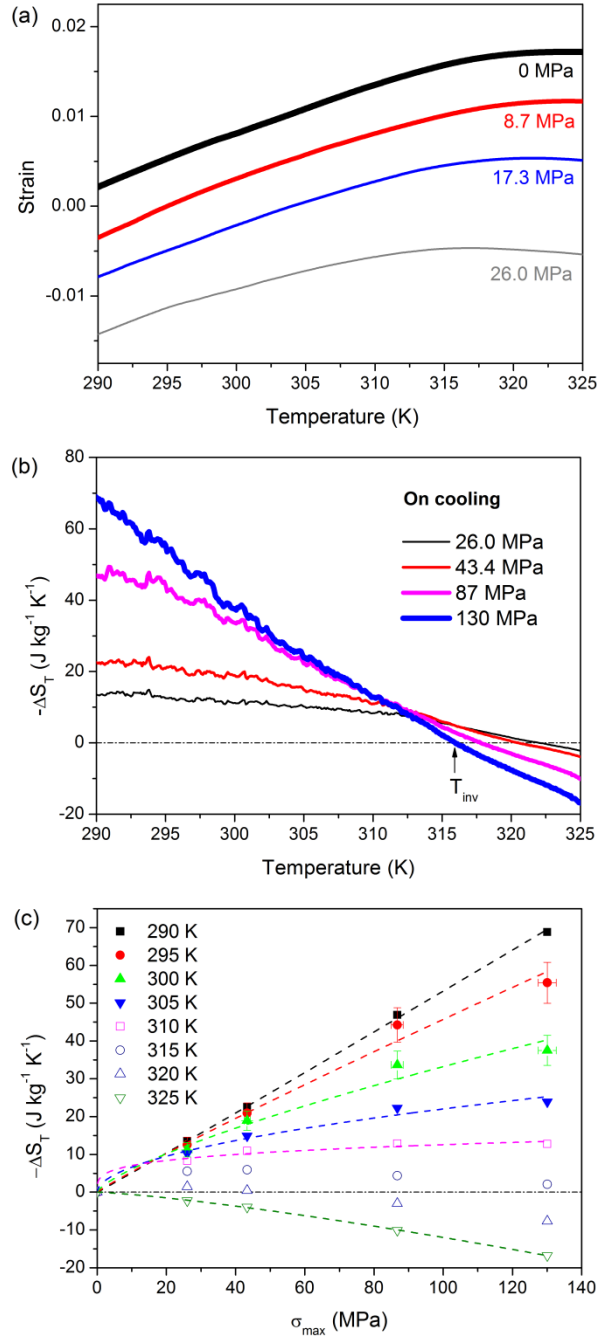


Fig. 3: (a) Strain (ϵ) vs. temperature (T) curves for PDMS at constant pressures of 0, 8.7(2), 17.3(3) and 26.0(5) measured on cooling, which were used to calculate the isothermal entropy change at $\Delta\sigma = 26.0(5)$

MPa; the other strain vs. temperature curves are shown in Fig 1 of *Supplementary information*. (b) Isothermal entropy change as a function of temperature for $\Delta\sigma = 26.0(5)$, 43.4(9), 87(2) and 130(3) MPa, obtained from ϵ vs. T data; the horizontal dash-dotted line at zero is a guide for the eyes; T_{inv} is the temperature that marks the inversion of the σ_b -CE (for 130(3) MPa as an example). (c) Isothermal entropy change vs. maximum applied pressure for different temperatures; the dotted lines are the fits using Eq. 3; the horizontal dash-dot line at zero is a guide for the eyes to separate the ordinary σ_b -CE from the σ_b -CE; the error bars (2% for σ_{max} and $1 \text{ J kg}^{-1} \text{K}^{-1} + 8\%$ for ΔS_T) were only shown for 295 and 300 K data for the sake of clarity.

In Fig. 3c, we show ΔS_T as a function of the maximum applied pressure (σ_{max}) for different temperatures. We fitted the ordinary σ_b -CE for different temperatures also using a power law as following:

$$-\Delta S_T(T, \sigma_{max}) = b\sigma_{max}^m, \quad (3)$$

where b is the constant of proportionality, and m is the power law exponent. For 290 K, $b = 0.55(2)$ kJ kg⁻¹ K⁻¹ GPa^{-m} and $m = 1.02(2)$; for 295 K, $b = 0.39(8)$ kJ kg⁻¹ K⁻¹ GPa^{-m} and $m = 0.9(1)$; for 300 K, $b = 0.18(5)$ kJ kg⁻¹ K⁻¹ GPa^{-m} and $m = 0.7(1)$; for 305 K, $b = 0.07(2)$ kJ kg⁻¹ K⁻¹ GPa^{-m} and $m = 0.5(1)$; for 310 K, $b = 0.022(4)$ kJ kg⁻¹ K⁻¹ GPa^{-m} and $m = 0.25(7)$; for 325 K, $b = -0.23(2)$ kJ kg⁻¹ K⁻¹ GPa^{-m} and $m = 1.29(3)$. It is easy to see that b and m decrease when the temperature increases for ordinary σ_b -CE. Furthermore, the power law works while $\left(\frac{d\Delta S_T}{d\sigma_{max}}\right)_T$ does not change the sign for the entire range of pressure (i.e., the power law fails for 315 and 320 K). The behavior of the power law parameters for entropy change (b and m) as well as the parameters for temperature change (a and n) need further investigation to be better understood.

In tractive σ_e -CE of natural rubber and synthetic rubber-like polymers at low stresses, ΔT values greater than 10 K requires large strain amplitudes of 400 - 700%^{14,29,30}. On the other hand, giant thermal σ_b -CE values (> 20 K) in SMAs are exhibited in small strain amplitudes, but often require high pressures (several hundreds of MPa)²⁵. Considering only these features (large strains or high pressures), hitherto, tractive σ_e -CE in polymers or σ_b -CE in intermetallics have presented significant limitations to be used in commercial cooling devices. Now, considering σ_b -CE in elastomer polymers, such as PDMS (giant ΔT , giant ΔS , $\sigma < 300$ MPa and $|\epsilon| < 20\%$), this scenario seems to change.

In order to compare the barocaloric properties of PDMS around room temperature with different relevant barocaloric materials from the literature^{11,17,31,32,33}, we present the *normalized temperature change* ($|\Delta T/\Delta\sigma|$) as a function of temperature (Fig. 4a). A remarkable $|\Delta T/\Delta\sigma|$ of ~ 70 K GPa⁻¹ was obtained for PDMS, which remains practically constant in a large temperature range. Comparing with other direct measurements, that value is larger or much larger than for any other promising barocaloric material recently reported. We also calculated the *normalized refrigerant capacity* ($NRC \equiv |RC/\Delta\sigma|$) as a function of the temperature difference between hot

reservoir and cold reservoir ($\Delta T_{h-c} \equiv T_{hot} - T_{cold}$). For PDMS, we fixed the hot reservoir at 315 K. It is noteworthy that NRC sharply increases as function of ΔT_{h-c} , surpassing $6 \text{ kJ kg}^{-1} \text{ GPa}^{-1}$ for $\Delta T_{h-c} = 25 \text{ K}$.

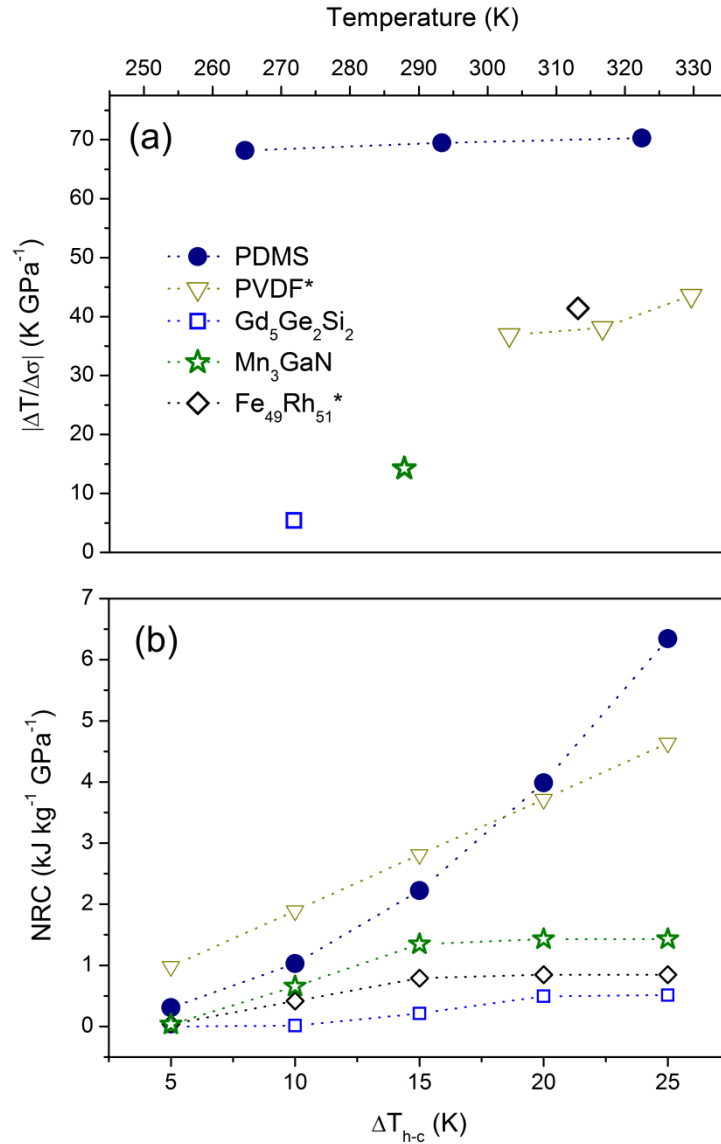


Fig. 4: Barocaloric properties for materials with large or giant σ_b -CE around room temperature (250 - 330 K). (a) Normalized temperature change ($|\Delta T / \Delta \sigma|$): PDMS ($|\Delta \sigma| = 173 \text{ MPa}$); PVDF ($|\Delta \sigma| = 150 \text{ MPa}$)¹⁷; Gd₅Ge₂Si₂ (maximum reported for $|\Delta \sigma| = 200 \text{ MPa}$)³¹; Mn₃GaN (maximum reported for $|\Delta \sigma| = 93 \text{ MPa}$)³²; Fe₄₉Rh₅₁ (maximum reported for $|\Delta \sigma| = 250 \text{ MPa}$)³³. *Indirect determination. (b) Normalized refrigerant capacity ($|\text{RC} / \Delta \sigma|$) as a function of $\Delta T_{h-c} \equiv T_{hot} - T_{cold}$ (temperature difference between hot reservoir and cold reservoir): PDMS ($T_{hot} = 315 \text{ K}$, $|\Delta \sigma| = 130 \text{ MPa}$); PVDF ($T_{hot} = 330 \text{ K}$, $|\Delta \sigma| = 150 \text{ MPa}$)¹⁷; Gd₅Ge₂Si₂ ($T_{hot} = 275 \text{ K}$, $|\Delta \sigma| = 150 \text{ MPa}$)³¹; Mn₃GaN ($T_{hot} = 295 \text{ K}$, $|\Delta \sigma| = 139 \text{ MPa}$)³²; Fe₄₉Rh₅₁ ($T_{hot} = 325 \text{ K}$, $|\Delta \sigma| = 160 \text{ MPa}$)¹¹.

In summary, we presented outstanding results concerning the barocaloric properties of PDMS rubber. The pressure-induced temperature changes are huge (e.g., at ~283 K, $\Delta T = -28.5$ K, for $\Delta\sigma = -390$ MPa; or $\Delta T = -22.4$ K, for $\Delta\sigma = -273$ MPa), as well as the isothermal entropy changes (e.g., $\Delta S_T = -69$ J kg⁻¹ K⁻¹ at 290 K, for only $\Delta\sigma = 130(3)$ MPa). Considering normalized parameters, PDMS exhibits the normalized temperature change $|\Delta T/\Delta\sigma| \approx 70$ K GPa⁻¹ from ~265 to ~322 K, and the normalized refrigerant capacity $NRC \approx 6.3$ kJ kg⁻¹ GPa⁻¹, for $\Delta T_{h-c} = 25$ K. Therefore, the extraordinary barocaloric effects observed at low pressures ($\Delta\sigma < 400$ MPa) and low strains ($|\varepsilon| < 20\%$) opens a promising road towards solid-state cooling based on elastomer polymers submitted to confined compression.

Methods

The PDMS samples were prepared from the commercial components supplied by Dow Corning[®]. The base elastomers were mixed with the cure agent (Sylgard 184) following the mass proportion of 10:1. To avoid air bubbles, the mixture was put in low vacuum for about 45 minutes. We used two metallic cylinders with two diameters (8 mm and 12 mm) as a mold for making the samples. The mixture was poured into the mold over a glass plate until it was completely filled and then placed on a hot plate (368 K) for 50 minutes. We made two samples with the following dimensions: 12 mm (diameter) and 17 mm (length); 8 mm (diameter) and 20 mm (length). The densities of the samples are 1026(3) and 1030(7) kg m⁻³, respectively. In the experiments performed in pressures up to 173 MPa, we used the same PDMS sample with 12 mm of diameter. For experiments above 173 MPa, the same 8-mm-diameter sample was used. We characterized the 12-mm-diameter sample via Fourier transform infrared spectroscopy (FTIR) from 450 to 4000 cm⁻¹, with a fixed step of 2 cm⁻¹ (Fig. 2 in *Supplementary information*), using a FTIR spectrometer from PerkinElmer[®] (model Spectrum Two).

The experimental setup consists of a cylinder carbon-steel chamber enveloped by a copper coil, which water or liquid nitrogen circulates inside for refrigerating/heating. For temperatures above 280 K, a thermostatic bath (TE 184, Tecnal) was used to pump water in the copper coil. For temperatures below 280 K, we used liquid nitrogen to refrigerate the sample. A set of two resistors (NP 38899, HG

Resistências) placed in the proper holes in the chamber helps to precisely control the temperature when used together with the liquid nitrogen. Two variations of the chamber were used: one with a 12-mm-diameter cylindrical hole and another one with a 8-mm-diameter cylindrical hole. Pistons with the respective diameters move through the cylindrical holes in the center of the chamber, where the sample is placed in. Below the sample, there is a bottom closure to hold the sample inside the chamber and to guide a thermocouple, whose tip is placed in the sample to measure its temperature in real time. Uniaxial load at the piston is applied by a manual hydraulic press (P15500, Bonevau). Underneath the system, a load cell (3101C, ALFA Instrumentos) measures the contact force. Finally, the displacement of the sample is measured with a rod attached to the piston by a precise linear length gauge (METRO 2500, Heidenhain Co). Temperatures are collected and controlled (when using the resistors) by Model 335, Lake Shore Cryotronics. A schematic view of the system is reported by Bom et al.³⁴.

The data for the direct temperature change (ΔT) were obtained by applying pressure very close to the adiabatic condition. When the temperature in the sample is stable, a compressive stress (maximum values in the range of 8.7 - 390 MPa) is applied rapidly, resulting in an immediate increase in temperature. The load is kept constant until the temperature decreases down to the initial temperature, and then the stress is released adiabatically, causing an abrupt decrease in the sample's temperature.

Strain vs. temperature experiments were performed at isobaric processes, i.e., the temperature was reduced under a constant pressure in the range of 8.7 - 130 MPa. Firstly, we set a temperature of 328 K in the sample, and then a compressive stress is applied and kept constant. Temperature is varied continuously between ~328 – 283 K performing the following cycle: 328 K \rightarrow 283 K \rightarrow 328 K \rightarrow 283 K.

References

1. Gough, J. A description of a property of caoutchouc or Indian rubber; with some reflections on the cause of the elasticity of this substance. *Mem. Lit. Phil. Soc. Manchester* 1 (2nd Series), 288–295 (1805).
2. Joule, J. P. On some thermo-dynamic properties of solids. *Phil. Trans. R. Soc. Lond.* 149, 91–131 (1859).

3. Thomson, W. (Lord Kelvin). On the thermoelastic, thermomagnetic, and pyroelectric properties of matter. *Lond. Edinb. Dublin Phil. Mag. J. Sci.* 5, 4–27 (1878).
4. Pecharsky, V. K. & Gschneidner Jr., K. A. Giant magnetocaloric effect in $\text{Gd}_5(\text{Si}_2\text{Ge}_2)$. *Phys. Rev. Lett.* 78, 4494–4497 (1997).
5. Mischenko, A. S. *et al.* Giant electrocaloric effect in thin-film $\text{PbZr}_{0.95}\text{Ti}_{0.05}\text{O}_3$. *Science* 311, 1270–1271 (2006).
6. Dart, S. L., Anthony, R. L. & Guth, E. Rise of temperature on fast stretching of synthetic and natural rubbers. *Ind. Eng. Chem.* 34, 1340–1342 (1942).
7. Dart, S. L. & Guth, E. Rise of temperature on fast stretching of butyl rubber. *Rubber Chem. Technol.* 18, 803–816 (1945).
8. Bonnot, E. *et al.* Elastocaloric effect associated with the martensitic transition in shape-memory alloys. *Phys. Rev. Lett.* 100, 125901 (2008).
9. Mañosa, L. *et al.* Giant solid-state barocaloric effect in the Ni–Mn–In magnetic shape-memory alloy. *Nat. Mater.* 9, 478–481 (2010).
10. Millán-Solsona, R. *et al.* Large entropy change associated with the elastocaloric effect in polycrystalline Ni–Mn–Sb–Co magnetic shape memory alloys. *Appl. Phys. Lett.* 105, 241901 (2014).
11. Stern-Taulats, E. *et al.* Barocaloric and magnetocaloric effects in $\text{Fe}_{49}\text{Rh}_{51}$. *Phys. Rev. B* 89, 214105 (2014).
12. Lloveras, P. *et al.* Giant barocaloric effects at low pressure in ferroelectric ammonium sulphate, *Nat. Commun.* 6, 8801 (2015).
13. Tušek, J. *et al.* A regenerative elastocaloric heat pump. *Nat. Energy*, 1, 16134 (2016).
14. Guyomar, D. *et al.* Elastocaloric modeling of natural rubber. *Appl. Therm. Eng.* 57, 33–38 (2013).
15. Xie, Z., Sebald, G. & Guyomar, D. Elastocaloric effect dependence on pre-elongation in natural rubber. *Appl. Phys. Lett.* 107, 081905 (2015).
16. Matsuo, T. *et al.* Mechanocaloric properties of poly(dimethylsiloxane) and ethylene–propylene rubbers. *J. Therm. Anal. Calorim.* 123, 1817–1824 (2016).
17. Patel, S. *et al.* Elastocaloric and barocaloric effects in polyvinylidene di-fluoride-based polymers. *Appl. Phys. Lett.* 108, 072903 (2016).
18. Xie, Z., Sebald, G. & Guyomar, D. Comparison of direct and indirect measurement of the elastocaloric effect in natural rubber. *Appl. Phys. Lett.* 108, 041901 (2016).

19. Yoshida, Y. *et al.* Elastocaloric effect in poly(vinylidene fluoride-trifluoroethylene-chlorotrifluoroethylene) terpolymer. *Appl. Phys. Lett.* 108, 242904 (2016).
20. Usuda, E. O., Bom, N. M. & Carvalho, A. M. G. Large barocaloric effects at low pressures in natural rubber. arXiv:1701.05237 (2017).
21. Sebald, G., Xie, Z. & Guyomar, D. Fatigue effect of elastocaloric properties in natural rubber. *Phil. Trans. R. Soc. A*, 374, 20150302 (2016).
22. Treloar, L. R. G. *The physics of rubber elasticity*. Clarendon Press: Oxford, 3rd ed., 11 (1975).
23. Gschneidner, K. A. & Pecharsky Jr., V. K. Magnetocaloric Materials. *Annu. Rev. Mater.* 30, 387–429 (2000).
24. Moya, X., Kar-Narayan, S. & Mathur, N. D. Caloric materials near ferroic phase transitions. *Nat. Mater.* 13, 439–50 (2014).
25. Lu, B. & Liu, J. Mechanocaloric materials for solid-state cooling. *Sci. Bull.* 60, 1638–1643 (2015).
26. Mañosa, L. & Planes A. Mechanocaloric effects in shape memory alloys. *Phil. Trans. R. Soc. A* 374, 20150310 (2016).
27. Smith, A. *et al.* Material challenges for high performance magnetocaloric refrigeration devices. *Adv. Energy Mater.* 2, 1288–1318 (2012).
28. Lu, S. G., *et al.* Electrocaloric effect in ferroelectric polymers. *Appl. Phys. A Mater. Sci. Process.* 107, 559–566 (2012).
29. Dart, S. L, Anthony, R. L & Guth, E. Rise of temperature on fast stretching of synthetics and natural rubbers. *Ind. Eng. Chem.* 34, 1340–1342 (1942).
30. Mitchell, J. C & Meier D. J. Rapid stress-induced crystallization in natural rubber. *Rubber Chem. Technol.* 42, 1420–1432 (1969).
31. Yuce, S. *et al.* Barocaloric effect in the magnetocaloric prototype $Gd_5Si_2Ge_2$. *Appl. Phys. Lett.* 101, 071906 (2012).
32. Matsunami, D. *et al.* Giant barocaloric effect enhanced by the frustration of the antiferromagnetic phase in Mn_3GaN . *Nat. Mater.* 14, 73–78 (2015).
33. Stern-Taulats, E. *et al.* Reversible adiabatic temperature changes at the magnetocaloric and barocaloric effects in $Fe_{49}Rh_{51}$. *Appl. Phys. Lett.* 107, 152409 (2015).
34. Bom, N. M. *et al.* Experimental setup for measuring the barocaloric effect in polymers: Application to natural rubber. arXiv:1612.08638 (2016), accepted for publication in Review of Scientific Instruments.

Acknowledgements

The authors acknowledge financial support from FAPESP (project number 2012/03480-0), CNPq, CAPES, LNLS and CNPEM. The authors also thank Francesco G. Carotti and Maria Helena O. Piazzetta for the support in the preparation of PDMS samples.